Synthesis of ethanol-soluble few-layer graphene nanosheets for flexible and transparent conducting composite films

2011 Nanotechnology 22 295606

(http://iopscience.iop.org/0957-4484/22/29/295606)

Nanotechnology **22** (2011) 295606 (8pp) doi:10.1088/0957-4484/22/29/295606

Synthesis of ethanol-soluble few-layer graphene nanosheets for flexible and transparent conducting composite films

D D Nguyen[1], N H Tai[1], Y L Chueh[1], S Y Chen[1], Y J Chen[1], W S Kuo[2], T W Chou[3], C S Hsu[4] and L J Chen[1]

[1] Department of Materials Science and Engineering, National Tsing-Hua University, Hsinchu 300, Taiwan, Republic of China
[2] Department of Aerospace and Systems Engineering, Feng-Chia University, Taichung 407, Taiwan, Republic of China
[3] Department of Mechanical Engineering, Center for Composite Materials, 126 Spencer Laboratory, University of Delaware, Newark, DE 19716, USA
[4] Department of Applied Chemistry, National Chiao-Tung University, 1001 University Road, Hsinchu 300, Taiwan, Republic of China

E-mail: nhtai@mx.nthu.edu.tw and ylchueh@mx.nthu.edu.tw

Received 23 March 2011, in final form 20 May 2011
Published 17 June 2011
Online at stacks.iop.org/Nano/22/295606

Abstract
We report a facile method of preparing few-layer graphene nanosheets (FLGs), which can be soluble in ethanol. Atomic force microscopy and high-resolution transmission electron microscopy studies reveal that FLGs have average thicknesses in the range of 2.6–2.8 nm, corresponding to 8–9 layers. A graphene/nafion composite film has a sheet resistance of 9.70 kΩ/sq at the transmittance of 74.5% (at 550 nm) while the nafion film on polyethylene terephthalate has a sheet resistance of 128 kΩ/sq at transmittance of 90.0%. For the cycling/bending test, almost no change in resistance was exhibited when the film was bent at an angle up to 140°, and no obvious deviation in resistance could be found after 100 bending cycles was applied. In addition, an FLGs-poly(3,4-ethylenedioxythiophene):poly(styrenesulfonate) composite layer was demonstrated as the effective hole transporting layer to improve the hole transporting ability in an organic photovoltaic device, with which the power conversion efficiency was enhanced from 3.10% to 3.70%. The results demonstrated the promising applications of FLGs on graphene-based electronics, such as transparent electrode and flexible conducting film.

S Online supplementary data available from stacks.iop.org/Nano/22/295606/mmedia

(Some figures in this article are in colour only in the electronic version)

1. Introduction

Graphene, an atomic thin layer with sp^2-hybridized carbon atoms tightly packed into a two-dimensional (2D) honeycomb structure, has recently attracted tremendous attention due to its novel properties [1]. More recently, few-layer graphene nanosheets (FLGs) are considered to be a class of graphene materials [1], namely 2D graphitic crystals, with properties varied systematically by the number of graphene layers. Experimental studies revealed that FLGs possess extraordinary electronic transport properties [2–7] and are applicable as transparent and conductive electrodes for solar cell or liquid crystal devices [8, 9]. Several approaches to synthesize graphene have been proposed from mechanical exfoliation of graphite, through segregation out of a mediated metal layer via gaseous or solid sources to the unzipping of carbon nanotubes. Among them, chemical routes are the most realistic approach with low cost for the large scale production of graphene. Commonly, graphite oxide (GO) prepared by harsh oxidation of graphite via the Hummer method is

utilized as the starting material for synthesis of graphene nanosheets [10, 11]. However, graphene nanosheets derived from GO usually consist of defects and disorder, resulting in poor electrical properties [12, 13]. In addition, the reduction of GO involves strong reductive agents, such as hydrazine or dimethyl hydrazine, which are highly toxic and dangerously unstable.

An alternative way to chemically synthesize single- and few-layer graphene nanosheets, which has less defects and thereby much better conductivity, is via exfoliation from expanded graphite (EG) using organic solvents, such as *N*,*N*-dimethylformamide (DMF), *N*-methylpyrrolidone (NMP), chloroform and 1,2,4-trichlorobenzene [9, 14, 15]. Nevertheless, these organic solvents are expensive, poisonous and require special care for handling. Accordingly, developing a simple method by exfoliating graphite or mildly oxidized graphite (e.g. expanded graphite) into graphene using environmental, user-friendly, inexpensive and commercially available solvents is imperative. In this regard, we propose an approach by refluxing EG with nitric acid (HNO_3) solution, followed by ultrasonicating in ammonia–ethanol solution and finally dispersing in ethanol to achieve FLGs. The advantages of this chemically synthetic approach are of simplicity without toxic chemical agents and harsh oxidation of graphite. In addition, HNO_3 treatment has been reported to be an effective way to achieve p-type doping of graphite materials, enabling high conductivity of FLGs [16, 17]. Meanwhile, these FLGs are soluble in ethanol without the support of a surfactant/stabilizer, which is an important factor for the preparation of graphene nanosheets from expanded graphite, thereby avoiding interfusion of detrimental foreign compounds during the fabrication of graphene-based electronics and composites [12, 18].

2. Experimental part

2.1. Preparation of expanded graphite (EG)

The approaches of chemical intercalation and exfoliation were employed for the preparation of expanded graphite [19]. Natural graphite flakes with a mesh-80 size were intercalated by immersing the flakes in a mixture of H_2SO_4/HNO_3 (3:2 by volume) for 15 min at ambient conditions. To treat 100 g of the natural graphite flakes, 500 ml of the mixture solution was applied. The graphite-intercalated compound was washed with distilled water, neutralized to a pH value of about 5–6 and then dried at 100 °C in an oven. Exfoliation was carried out by introducing the graphite-intercalated compound in a preheated furnace at 1000 °C for 10 s. The thermal shock vaporizes the intercalation in the compound, providing the necessary force to overcome the van der Waals forces between graphene sheets. The intercalation and exfoliation of the natural graphite flakes result in EG, which is composed of partially connected graphite nanosheets with typical thicknesses in the range of 20–50 nm.

2.2. Preparation of few-layer graphene nanosheets (FLGs)

The expanded graphite (EG) was refluxed with concentrated HNO_3 acid at 80 °C for 36 h to covalently attach carboxylic groups on graphite edges. The acid-modified EG was then filtered and repeatedly washed with DI water until neutralized and dried at 80 °C to remove moisture. Subsequently, 40 mg of acid-modified EG was ultrasonicated in 180 ml mixture of NH_4OH:C_2H_5OH (8:1, v/v) for 3 h. This treatment results in the esterification of the carboxylic groups on graphite edges. The resultant mixture was then filtered through a polytetrafluoroethylene (PTFE) membrane (0.2 μm pore size) and washed with an excess amount of ethanol to completely remove the ammonia. The powder product remained on the membrane herein is named as functionalized EG. FLG dispersion was achieved by dispersing functionalized EG in ethanol utilizing a commercial ultrasonic cleaner (Bransonic) for 90 min, followed by settling the dispersion for one day, and finally decanting the supernatant of the dispersion. The solubility of FLGs in ethanol is 42 mg l^{-1}, determined by filtering the FLG dispersion through a pre-weighed 0.2 μm PTFE membrane.

2.3. Characterizations

FTIR spectra of EG, acid-modified EG and FLG samples (in powder form) were measured using a Perkin Elmer Spectrum RXI spectrometer. The UV–vis absorption spectra of FLG dispersions were measured by a U-3900H (Hitachi) spectrophotometer. A Horiba Jobin Yvon LabRam HR800 Raman microscope with excitation wavelength of 632.8 nm was used to distinguish the evolution from graphite to few-layer graphene. The sheet resistance and transmittance of the composite films were measured using the two-point method and the U-3900H spectrometer, respectively.

2.4. Fabrication of photovoltaic device

The organic photovoltaic devices were fabricated on ITO-coated glass substrates, which had been treated in acetone and isopropyl alcohol by an ultrasonic cleaner, followed by UV–ozone treatment. For fabrication of FLG–PEDOT:PSS composite layers, FLG powder derived from FLG dispersions in ethanol was dried at 80 °C in vacuum and was then dispersed in DMF solvent at a concentration of 40 mg l^{-1}. The resultant FLG dispersion was mixed with PEDOT:PSS at different volume ratios. A thin layer of FLG–PEDOT:PSS composite films was spin-coated onto the ITO glass at 400 rpm (rpm: revolutions per minute) for 5 s and then 2500 rpm for 40 s. The samples were dried at 120 °C for 30 min in vacuum and subsequently transferred into a nitrogen-filled glove box for spin-coating of a P_3HT:PCBM photoactive layer. The Ca (35 nm) and Al (150 nm) electrodes were thermally evaporated through a shadow mask with an active area of ∼1.0 cm^2. All the electrical measurements were performed in a glove box at room temperature.

3. Results and discussion

The expanded graphite was used as the starting material to prepare FLGs (see section 2 for more details). Due to the difference in surface tension between ethanol (∼22 mJ m^{-2})

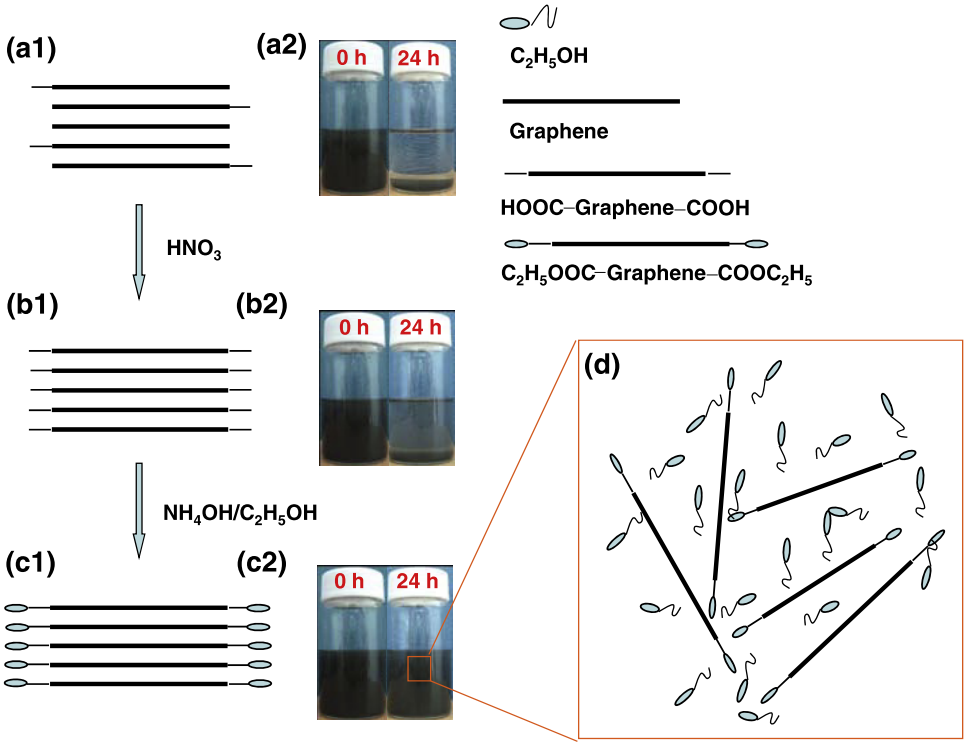

Figure 1. Schematic illustration of ethanol-soluble FLGs prepared using ammonia–ethanol treatment: (a1) EG, (b1) acid-modified EG, (c1) functionalized EG and (d) FLG dispersion in ethanol. Photos show dispersions of the (a2) EG, (b2) acid-modified EG and (c2) functionalized EG, respectively, before and after 24 h.

and the graphene layer (40–50 mJ m^{-2}), the wettability between EG and ethanol solvent is very poor [14]. The poor wettability makes ethanol molecules not easily intercalated into the interlayer of EG during the exfoliation process, leading to difficulty in exfoliating EG in graphene nanosheets. To overcome this problem, the functional group is used to anchor upon graphene edges by chemical treatment to assist the ultrasonic exfoliation of EG into graphene sheets. Overall processes of exfoliating EG into graphene are schematically illustrated in figure 1. First, EG (figure 1(a1)) was modified by HNO_3 solution to enrich the carboxylic group (–COOH) (figure 1(b1)). Subsequently, ammonia–ethanol solution (8:1, v/v) was used to anchor the functional $–COOC_2H_5$ group onto graphene edges through the esterification reaction of the –COOH group while a layered morphology still remains, as schematically shown in figure 1(c1). Finally, larger scale FLGs can be synthesized by simple ultrasonication of the functionalized EG. Note that the FLGs with functional groups are soluble in ethanol as schematically shown in figure 1(d). The chemical modification of EG can be clearly distinguished from Fourier transform infrared spectra, as shown in figures 2(a)–(c), for three kinds of samples, namely EG, acid-modified EG and FLGs, respectively. Two distinct transmittance peaks for EG at ∼1100 and 1640 cm^{-1}, corresponding to vibration modes of C–C–O and C=O, respectively, can be found [20]. After treatment with nitric acid at 80 °C for 36 h to covalently attach the –COOH group on graphene edges, the peak intensity of C=O at 1640 cm^{-1} was increased and a new peak at 1380 cm^{-1} originating from C–OH was found, providing evidence of the –COOH group [21–23]. The increase of intensity and up-shift (from 1530 to 1565 cm^{-1}) of C=C peaks in the spectrum of FLG, as compared with that of EG, are due to the addition of localized C=C bonds [20], which are generated through the opening of the carbon ring structure during the ultrasonic exfoliation process. While in the FTIR spectrum of acid-modified EG, the C=C peak is not obvious because of the predominant C=O and C–OH peaks in the –COOH groups. The functional group $–COOC_2H_5$ was found in the FLG sample due to the appearance of the C–H bond at 1465 cm^{-1}, which is attributed to bending vibrations from the $–CH_3$ group after esterification of the carboxylic groups on graphene edges in an ammonia–ethanol solution [24, 25]. The introduction of the $–COOC_2H_5$ group is believed to increase the wettability between graphene layers and ethanol, facilitating the intercalation of ethanol molecules into the interlayer of EG to decrease van der Waals force interactions. Therefore, few-layer graphene can be straightforwardly exfoliated from functionalized EG by ultrasonication and uniformly dispersed in ethanol.

To evaluate the effectiveness of the proposed method, EG, acid-modified EG and functionalized EG were dispersed in ethanol as shown in figures 1(a2)–(c2). Obviously, segregation at the bottom of glass vials was clearly observed for two EG samples with and without acid modification when the settled time exceeds 24 h. In contrast, the dispersion derived from the functionalized EG is still opaque, indicating the stable dispersion, even the settled time was over two weeks. The compatibility of the functionalized EG with ethanol was further

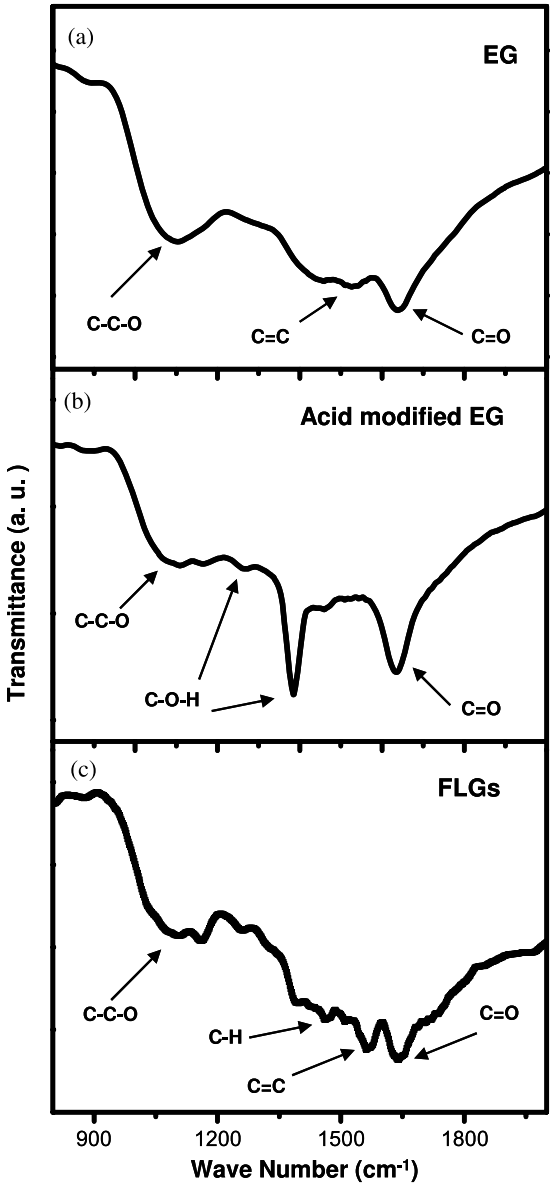

Figure 2. Fourier transform infrared spectra of (a) EG, (b) acid-modified EG and (c) FLGs.

demonstrated by dispersing it into a water–ethanol mixture at various volume ratios (see supporting information, figure S1 available at stacks.iop.org/Nano/22/295606/mmedia). The dispersion of functionalized EG is completely soluble and stable in the ethanol solvent while its stability decreases as the volume ratio of water increases in the solutions and becomes completely hydrophobic to water. Furthermore, FLGs derived from functionalized EG were also found to be soluble in other solvents, such as DMF, NMP, tetrahydrofuran and chloroform, thereby facilitating its capacity of incorporating into a variety of polymer matrices as graphene-based composites.

Absorption spectroscopy can be used to further shed light on how uniform FLGs are in ethanol. The absorption spectra are acquired by a UV–visible spectrometer with a wavelength of 250–850 nm at different concentrations of FLGs from 12 to 42 mg l^{-1}, as shown in figure 3(a). All spectra show a distinct absorption peak at 268 nm, which is related to the electronic π–π^* transition of C=C bonds. As can be seen, the intensity of absorption spectra at 268 nm increases with the FLG concentration. A linear relationship is shown in the inset of figure 3(a), following the Lambert–Beer law [26]. Thus, the absorption coefficient (at 268 nm) ε of ~1371 L g^{-1} m^{-1} can be extracted from the equation $A = \varepsilon LC$, where A is absorption intensity, L is the distance the light travels through FLG dispersions and C is the concentration of FLG dispersions. Figure 3(b) shows the Raman spectra of EG, acid-modified EG and FLGs, respectively, with which the He–Ne laser was used as the light source at the wavelength of 632.8 nm. Two characteristic peaks at 1580 and 2690 cm^{-1}, corresponding to the G and the 2D bands, respectively, can be observed for all samples, which result from the E_{2g} vibrational mode of sp^2-bonded carbon and the second-order vibration caused by the scattering of phonons at the zone boundary [27, 28]. For the FLG sample, a peak at 1330 cm^{-1}, corresponding to the D band, appears, which is associated with disordered sp^3-hybridized carbon such as defects or impurities in carbon materials [28]. No remarkable difference is observed for EG and acid-modified EG samples, indicating that the acid treatment does not damage the graphitic quality of the acid-modified EG sample. Noting that a significant change in spectrum and blueshift δ_λ of 25.8 cm^{-1} at the 2D peak is evidence of the evolution from graphite to FLG [27–29]. To measure the thickness of an individual sheet FLG by atomic force microscopy (AFM), the FLG dispersion was drop-cast onto an SiO_2/Si substrate. A typical AFM image of FLGs on an SiO_2/Si substrate is shown in figure 3(c). The uniformly distributed individual FLG sheets with grain sizes up to several microns indicate the well-dispersed FLGs in ethanol solvent. Moreover, the distribution of FLG thicknesses ranged from 2.2 to 3.2 nm with an average thickness of ~2.7 nm was obtained by taking 100 FLGs into account as shown in the inset of figure 3(c). Figure 3(d) shows a typical AFM image of the FLG taken from the rectangular area of figure 3(c), distinctly revealing a very smooth surface with a thickness of 2.6 nm, corresponding to 8–9 graphene layers, which is consistent with the high-resolution TEM image (see supporting information, figure S2 available at stacks.iop.org/Nano/22/295606/mmedia.)

Both ethanol-soluble and high conductive natures of the fabricated FLGs facilitate the incorporation of FLGs with a nafion polymer solution as a so-called graphene-based composite for the application in flexible electronics. The graphene-based composite possesses remarkable enhancement in electrical and mechanical properties compared to the host materials. To investigate in depth the graphene-based composite as the transparent conductor, FLG films with different thicknesses (by controlling different volumes of FLG dispersions) were first prepared from FLG dispersions via vacuum filtration using an anodic membrane as the filter (Whatman, 0.1 μm pore size) and followed by transferring FLG films onto a nafion conductive layer, which were spin-coated on a polyethylene-terephthalate (PET) substrate as the transfer medium. Figure 4(a) reveals the transmittance spectra and sheet resistances of the nafion film and the FLG/nafion

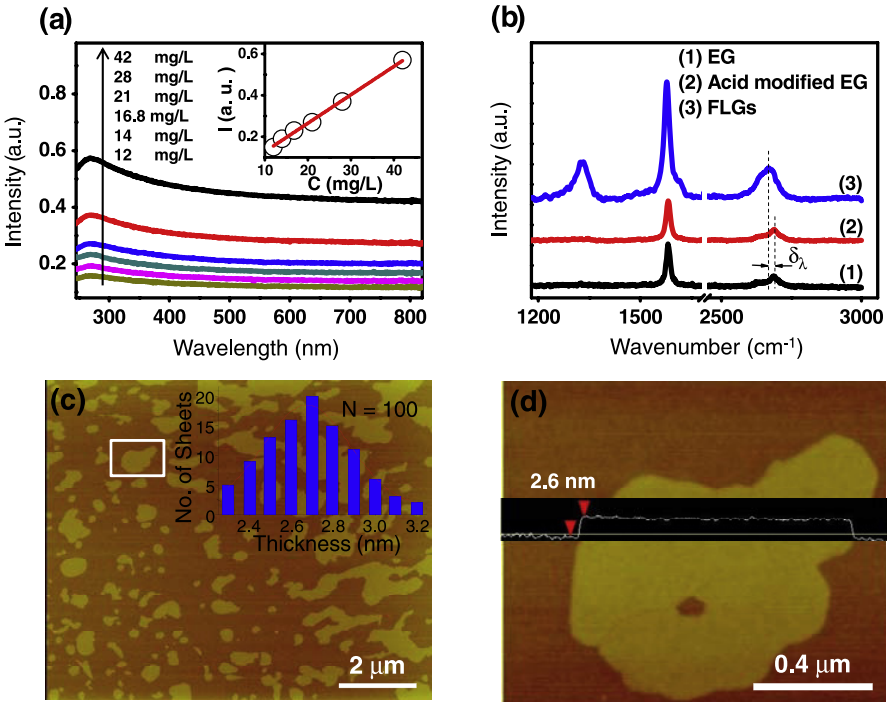

Figure 3. UV–vis spectra of FLG dispersion at different concentrations. Inset is a plot of absorption intensity versus FLG concentration (a); Raman spectra (b) of EG (1), acid-modified EG (2) and FLGs (3), respectively; a typical AFM image of FLGs on SiO_2 substrate: inset is thickness distribution of 100 sheets (c) and AFM image of a single FLG with smooth planar structure (d).

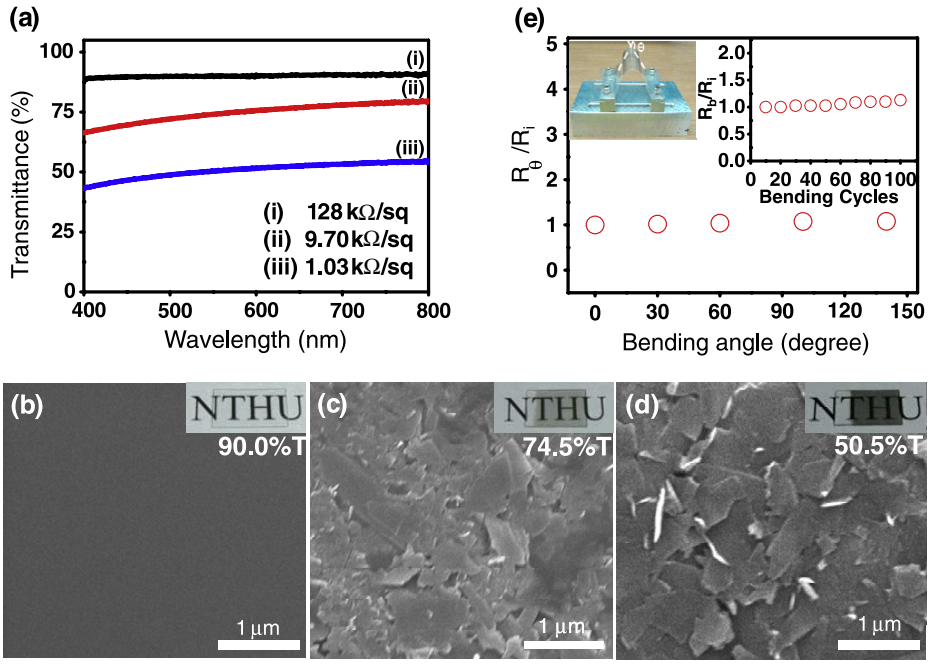

Figure 4. Optical transmission spectra (a) of nafion film (i) and FLG/nafion films (ii, iii) on PET substrates, respectively; and corresponding SEM images of nafion (b) and FLG/nafion films with different FLG contents ((c), (d)); bending test of an FLG/nafion film on PET, right inset is a plot of electrical resistance change versus number of bending cycles, left inset is experimental configuration for bending test (e).

films on PET substrates. The corresponding SEM images of the nafion film and the two different graphene-based composite films from low to high volume ratio of FLGs and nafion are shown in figures 4(b)–(d). Insets in figures 4(b)–(d) reveal the photo images of each sample, demonstrating the transparent property. Although a high transmittance of 90.0% of pure nafion film on PET at the wavelength of 550 nm can be achieved, however, the sheet resistance of 128 kΩ/sq is high, which limits the application as a transparent electrode. After transferring FLGs onto nafion film as a graphene/nafion

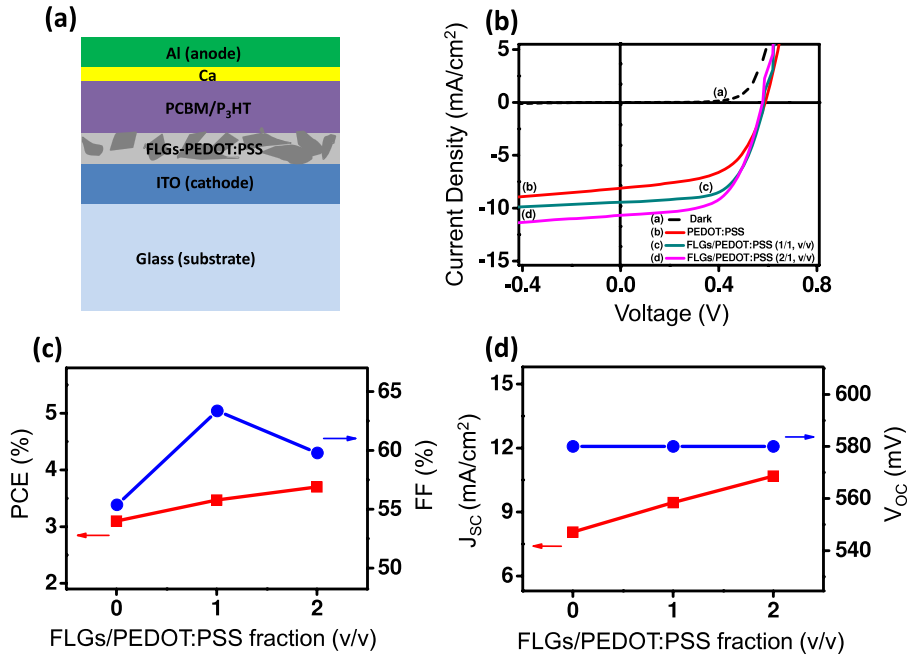

Figure 5. Structure of organic photovoltaic device with the incorporation of FLG–PEDOT:PSS composite layer (a); I–V characteristics (b), power conversion efficiency and fill factor (c), and short circuit current and open circuit voltage (d) of photovoltaic devices with FLG–PEDOT:PSS composite layer at different volume ratios.

composite layer, the sheet resistance is significantly reduced by over one order of magnitude but the transmittance is only decreased from 90.0% to 74.5%. By further increasing FLG content in the graphene/nafion composite film, the film with a sheet resistance of up to 1.03 kΩ/sq can be achieved while the transmittance is decreased to 50.5%. Compared with the sheet resistance of 33.4 kΩ/sq and transmittance of 72.8% (at 550 nm) of a conventional graphene-based composite film prepared directly from an FLG–nafion mixed solution, the FLG/nafion bilayer structure achieves lower sheet resistance. The reason is due to that the conductive paths of electrons are mainly through FLGs rather than the nafion layer since the nafion layer only acts as a secondary path for electron transfer, thereby enhancing the conductivity. To realize the application of the FLG/nafion composite layer as a transparent electrode in flexible devices, an understanding of the electromechanical properties of FLGs/nafion composite films is imperative. Figure 4(e) shows electrical resistance behavior of an FLGs/nafion composite film under different bending angles which are defined as the angles of intersections drawn from two bent ends. The overall configuration of electromechanical measurements is shown in the left inset of figure 4(e). The resistance of the FLG/nafion composite film is almost unchanged even for a bent angle exceeding 140°. Furthermore, after bending 100 cycles (right inset in figure 4(e)), the deviation of the resistance is not severe, exhibiting excellent mechanical flexibility of the FLGs/nafion composite film.

To demonstrate the application of our graphene-based composite film in a photovoltaic device, we used a graphene–poly(3,4-ethylenedioxythiophene):poly(styrenesulfonate) (PEDOT:PSS) composite film as an efficient hole transporting layer. It has been reported that acid-oxidized multi-wall carbon nanotubes (MWCNTs) can enhance the transportation of holes to increase the efficiency of the photovoltaic devices when introducing them to the PEDOT:PSS [30–33]. With this regard, we mixed FLGs with PEDOT:PSS at different volume ratios and studied its hole transport property in the well-known organic photovoltaic device, namely a bulk heterojunction architecture based on poly(3-hexylthiophene) (P_3HT) and fullerene derivative phenyl-C61-butyric acid methyl ester (PCBM). The structure of the device with the incorporation of an FLG–PEDOT:PSS composite layer is shown in figure 5(a). All samples were measured under the light illumination of AM 1.5 (100 mW cm^{-2}). Figure 5(b) shows the current–voltage (I–V) characteristics for pure PEDOT:PSS and FLG–PEDOT:PSS composite layers with different volume ratios. The corresponding filling factor (FF) and power conversion efficiency (PCE), and short circuit current density (J_{SC}) and open circuit voltage (V_{OC}), are shown in figures 5(c) and (d), respectively. Obviously, for the device adopting only PEDOT:PSS yields J_{SC} of 8.06 mA cm^{-2}, V_{OC} of 0.58 V, FF of 55.37% and PCE of 3.10% while for the device comprised of FLG–PEDOT:PSS composite layers, J_{SC} and PCE can be enhanced from 8.06 to 9.44 mA cm^{-2} and 3.10 to 3.47%, respectively, at the mixed FLGs/PEDOT:PSS volume (v/v) of 1/1. By increasing the v/v ratio of FLGs and PEDOT:PSS to 2/1, the J_{SC} and PCE can further increase to 10.68 mA cm^{-2} and 3.70%, respectively. Noting that the V_{OC} of all devices are the same (0.58 V), indicating that the energy band alignment within mixed PCBM and P_3HT is not influenced by FLG–PEDOT:PSS composite layers. Due to partially containing oxygen groups on the graphene edges of FLGs, it is expected that the work function of the FLGs is in the range of 4.4 eV (graphite) to 5.1 eV (acid-oxidized MWCNTs), therefore possessing an energy level close to that of P_3HT

(4.65–4.85 eV) [34, 35]. Furthermore, no significant differences were found in surface roughness between the pure PEDOT:PSS and the FLG–PEDOT:PSS composite films, indicating that the contact resistance between the active layer and the hole transport layer is unchanged in all devices (see supporting information, figure S3 available at stacks.iop.org/Nano/22/295606/mmedia). As a result, the significant improvement of current density is attributed to higher hole mobility of FLGs as compared with PEDOT:PSS, resulting in enhancing the probability of hole collection, thereby increasing device performance. The PEDOT:PSS performs in the device as a barrier of electron transfer while FLGs provide the function of rapid hole transfer. However, further studies need be carried out to find the mechanism of FLG–PEDOT:PSS composite film as the effective hole transport layer for photovoltaic devices. In addition, it has been reported that the acidic solvent and water molecular inside PEDOT:PSS can damage the ITO layer at elevated temperature [36, 37]. Our FLG–PEDOT:PSS composite films can also provide the advantage of reducing the damage of the ITO layer, as a result, enhancing the lifespan of the device.

4. Conclusions

In summary, we have developed a simple and effective method to prepare the dispersion of few-layer graphene nanosheets by ultrasonic treatment of acid-modified expanded graphite in an ammonia–ethanol solution. Few-layer graphene nanosheets with 8–9 layers and a lateral size up to several micrometers were synthesized. The ethanol solvent with low boiling point facilitates the deposition of graphene nanosheets individually on various surfaces, thus leading to applications in graphene-based electronics. A graphene/nafion composite film has a sheet resistance of 9.70 kΩ/sq at the transmittance of 74.5% (at 550 nm) while the nafion film on PET has a sheet resistance of 128 kΩ/sq at transmittance of 90.0%. For the cycling/bending test, almost no change in resistance is exhibited when the film was bent at angles up to 140°, and no obvious deviation in resistance can be found after 100 bending cycles is applied. In addition, an FLG–PEDOT:PSS composite layer was demonstrated as the effective hole transporting layer to improve the hole transporting ability in organic photovoltaic devices with an enhanced PCE from 3.10% to 3.70%.

Acknowledgments

This research was supported by the National Science Council under grant nos. 98-2221-E-007-045-MY3, 100-ET-EE-007-003-ET and NSC 98-2112-M-007-025-MY3.

References

[1] Geim A K and Novoselov K S 2007 The rise of graphene *Nat. Mater.* **6** 183
[2] Lee J H, Shin D W, Makotchenko V G, Nazarov A S, Fedorov V E, Yoo J H, Yu S M, Choi J Y, Kim J M and Yoo J B 2010 The superior dispersion of easily soluble graphite *Small* **6** 58
[3] Lee J H, Shin D W, Makotchenko V G, Nazarov A S, Fedorov V E, Kim Y H, Choi J Y, Kim J M and Yoo J B 2009 One-step exfoliation synthesis of easily soluble graphite and transparent conducting graphene sheets *Adv. Mater.* **21** 4383
[4] Berger C *et al* 2004 Ultrathin epitaxial graphite: 2D electron gas properties and a route toward graphene-based nanoelectronics *J. Phys. Chem.* B **108** 19912
[5] Srivastava A, Galande C, Ci L, Song L, Rai C, Jariwala D, Kelly K F and Ajayan P M 2010 Novel liquid precursor-based facile synthesis of large-area continuous, single, and few-layer graphene films *Chem. Mater.* **22** 3457
[6] Cai W, Zhu Y, Li X, Piner R D and Ruoff R S 2009 Large area few-layer graphene/graphite films as transparent thin conducting electrodes *Appl. Phys. Lett.* **95** 123115
[7] Reina A, Jia X, Ho J, Nezich D, Son H, Bulovic V, Dresselhaus M S and Kong J 2009 Large area, few-layer graphene films on arbitrary substrates by chemical vapor deposition *Nano Lett.* **9** 30
[8] Wang X, Zhi L and Mullen K 2008 Transparent, conductive graphene electrodes for dye-sensitized solar cells *Nano Lett.* **8** 323
[9] Blake P *et al* 2008 Graphene-based liquid crystal device *Nano Lett.* **8** 1704
[10] Stankovich S, Dikin D A, Piner R D, Kohlhaas K A, Kleinhammes A, Jia Y, Wu Y, Nguyen S B T and Ruoff R S 2007 Synthesis of graphene-based nanosheets via chemical reduction of exfoliated graphite oxide *Carbon* **4** 1558
[11] Schniepp H C, Li J L, McAllister M J, Sai H, Alonso M H, Adamson D H, Prud'homme R K, Car R, Saville D A and Aksay I A 2006 Functionalized single graphene sheets derived from splitting graphite oxide *J. Phys. Chem.* B **110** 8535
[12] Li X, Zhang G, Bai X, Sun X, Wang X, Wang E and Dai H 2008 Highly conducting graphene sheets and Langmuir–Blodgett films *Nat. Nanotechnol.* **3** 538
[13] Becerril H A, Mao J, Liu Z, Stoltenberg R M, Bao Z and Chen Y 2008 Evaluation of solution-processed reduced graphene oxide films as transparent conductors *ACS Nano* **2** 463
[14] Hernandez Y *et al* 2008 High-yield production of graphene by liquid-phase exfoliation of graphite *Nat. Nanotechnol.* **3** 563
[15] Chattopadhyay J, Mukherjee A, Chakraborty S, Kang J H, Loos P J, Kelly K F, Schmidt H K and Billups W E 2009 Exfoliated soluble graphite *Carbon* **47** 2945
[16] Fillaux F, Menu S, Conard J, Fuzellier H, Parker S W, Hanon A C and Tomkinson J 1999 Inelastic neutron scattering study of the proton dynamics in HNO_3 graphite intercalation compounds *Chem. Phys.* **242** 273
[17] Kasry A, Kuroda M A, Martyna G J, Tulevski G S and Bol A A 2010 Chemical doping of large-area stacked graphene films for use as transparent, conducting electrodes *ACS Nano* **4** 3839
[18] Hao R, Qian W, Zhang L and Hou Y L 2008 Aqueous dispersions of TCNQ-anion-stabilized graphene sheets *Chem. Commun.* 6576
[19] Kuo W S and Lu H F 2008 Bending fracture in carbon nanotubes *Nanotechnology* **19** 495710
[20] Kim U J, Furtado C A, Liu X, Chen G and Eklund P C 2005 Raman and IR spectroscopy of chemically processed single-walled carbon nanotubes *J. Am. Chem. Soc.* **127** 15437
[21] Stankovich S, Piner R D, Nguyen S B T and Ruof R S 2006 Synthesis and exfoliation of isocyanate-treated graphene oxide nanoplatelets *Carbon* **44** 3342
[22] Bourlinos A B, Gournis D, Petridis D, Szabó T, Szeri A and Dékány I 2003 Graphite oxide: chemical reduction to graphite and surface modification with primary aliphatic amines and amino acids *Langmuir* **19** 6050

[23] Ying Z, Lin X, Qi Y and Luo J 2008 Preparation and characterization of low-temperature expandable graphite *Mater. Res. Bull.* **43** 2677
[24] Chu B T T, Tobias G, Salzmann C G, Ballesteros B, Grobert N, Todd R I and Green M L H 2008 Fabrication of carbon-nanotube-reinforced glass–ceramic nanocomposites by ultrasonic *in situ* sol–gel processing *J. Mater. Chem.* **18** 5344
[25] Li Q, Kinloch I A and Windle A H 2005 Discrete dispersion of single-walled carbon nanotubes *Chem. Commun.* 3283
[26] Ingle J D J and Crouch S R 1988 *Spectrochemical Analysis* (Englewood Cliffs, NJ: Prentice Hall) p 372
[27] A C Ferrari *et al* 2006 Raman spectrum of graphene and graphene layers *Phys. Rev. Lett.* **97** 187401
[28] Malard L M, Pimenta M A, Dresselhaus G and Dresselhaus M S 2009 Raman spectroscopy in graphene *Phys. Rep.* **473** 51
[29] Chae S J *et al* 2009 Synthesis of large-area graphene layers on poly-nickel substrate by chemical vapor deposition: wrinkle formation *Adv. Mater.* **21** 2328
[30] Ago H, Petritsch K, Shaffer M S P, Windle A H and Friend R H 1999 Composites of carbon nanotubes and conjugated polymers for photovoltaic devices *Adv. Mater.* **11** 1281
[31] Pradhan B, Batabyal S K and Pal A J 2006 Functionalized carbon nanotubes in donor/acceptor-type photovoltaic devices *Appl. Phys. Lett.* **88** 093106
[32] Kalita G, Adhikari S, Aryal H R, Umeno M, Afre R, Soga T and Sharon M 2008 Fullerene (C_6O) decoration in oxygen plasma treated multiwalled carbon nanotubes for photovoltaic application *Appl. Phys. Lett.* **92** 063508
[33] Khatri I, Adhikari S, Aryal H R, Soga T, Jimbo T and Umeno M 2009 Improving photovoltaic properties by incorporating both single walled carbon nanotubes and functionalized multiwalled carbon nanotubes *Appl. Phys. Lett.* **94** 093509
[34] Ago H, Kugler T, Cacialli F, Salaneck W R, Shaffer M S P, Windle A H and Friend R H 1999 Work functions and surface functional groups of multiwall carbon nanotubes *J. Phys. Chem.* B **103** 8116
[35] Cascio A J, Lyon J E, Beerbom M M, Schlafa R, Zhu Y and Jenekhe S A 2006 Investigation of a polythiophene interface using photoemission spectroscopy in combination with electrospray thin-film deposition *Appl. Phys. Lett.* **88** 062104
[36] Kim Y H, Lee S H, Noh J and Han S H 2006 Performance and stability of electroluminescent device with self-assembled layers of poly(3,4-ethylenedioxythiophene)–poly(styrenesulfonate) and polyelectrolytes *Thin Solid Films* **510** 305
[37] Lagemaat J, Barnes T M, Rumbles G, Shaheen S E, Coutts T J, Weeks C, Levitsky I, Peltola J and Glatkowski P 2006 Organic solar cells with carbon nanotubes replacing In_2O_3:Sn as the transparent electrode *Appl. Phys. Lett.* **88** 233503